





Article

# Contribution of the Multiplicity Fluctuation in the Temperature Dependence of Phonon Spectra of Rare-Earth Cobaltites

Yuri S. Orlov <sup>1,2,\*</sup>, Alexey E. Sokolov <sup>1,2</sup>, Vyacheslav A. Dudnikov <sup>1</sup>, Karina V. Shulga <sup>2</sup>, Mikhail N. Volochaev <sup>1</sup>, Sergey M. Zharkov <sup>1,2</sup>, Nikolay P. Shestakov <sup>1</sup>, Maxim A. Vysotin <sup>1</sup> and Sergei G. Ovchinnikov <sup>1,2</sup>

<sup>1</sup> Kirensky Institute of Physics, Federal Research Center KSC SB RAS, 660036 Krasnoyarsk, Russia; alexeys@iph.krasn.ru (A.E.S.); slad63@yandex.ru (V.A.D.); volochaev91@mail.ru (M.N.V.); zharkov@iph.krasn.ru (S.M.Z.); nico@iph.krasn.ru (N.P.S.); mav@iph.krasn.ru (M.A.V.); sgo@iph.krasn.ru (S.G.O.)

<sup>2</sup> Institute of Engineering Physics and Radio Electronics, Siberian Federal University, 660041 Krasnoyarsk, Russia; tabakaewa-karina@mail.ru

\* Correspondence: jso.krasn@mail.ru

Academic Editor: Dawid Pinkowicz

Received: 1 September 2020; Accepted: 17 September 2020; Published: 20 September 2020



**Abstract:** We have studied, both experimentally and theoretically, the unusual temperature dependence of the phonon spectra in NdCoO<sub>3</sub>, SmCoO<sub>3</sub> and GdCoO<sub>3</sub>, where the Co<sup>3+</sup> ion is in the low-spin (LS) ground state, and at the finite temperature, the high-spin (HS) term has a nonzero concentration  $n_{HS}$  due to multiplicity fluctuations. We measured the absorption spectra in polycrystalline and nanostructured samples in the temperature range 3–550 K and found a quite strong breathing mode softening that cannot be explained by standard lattice anharmonicity. We showed that the anharmonicity in the electron–phonon interaction is responsible for this red shift proportional to the  $n_{HS}$  concentration.

**Keywords:** rare-earth cobalt oxides; multiplicity fluctuations; phonon spectra

## 1. Introduction

The close-to-spin crossover (SCO) of the high-spin (HS) and the low-spin (LS) terms of a magnetic cation, the energy of the multiplicity fluctuation  $\Delta_S = E_{HS} - E_{LS}$ , is small. The phenomenon of SCO in 3d-metal oxides is usually realized under high pressure [1], while in metal–ligand complexes in an organic matrix, the SCO may be induced by changing temperature [2–5]. There is also one more group of 3d-metal oxides, the rare-earth cobaltites RCoO<sub>3</sub> with a perovskite structure, very close to SCO [6–10]. The Co<sup>3+</sup> ion is in the LS ground state for all rare-earth ions, with very small energy  $\Delta_S \sim 100$  K for La. More-heavy rare-earth ions with smaller ionic radii have large energy  $\Delta_S$  [8,11]. With heating, the thermal excitation over the gap  $\Delta_S$  HS states results in a smooth change in structural, electronic, magnetic and thermodynamic properties; see [12] and the review [13]. Recently, we studied the effect of multiplicity fluctuation in cobalt ions on the crystal structure and magnetic and electrical properties of NdCoO<sub>3</sub> and SmCoO<sub>3</sub> [14], in comparison with GdCoO<sub>3</sub> [12]. The effect of multiplicity fluctuation on lattice vibration has not received much attention in the literature, while the large (about 10%) ionic-radius difference for the HS and LS states certainly may result in a change in the metal–ligand vibrations. Here, we study this effect by optical spectrum measurements in NdCoO<sub>3</sub>, SmCoO<sub>3</sub> and GdCoO<sub>3</sub> at different temperatures. We compare optical spectra in two types of samples, polycrystalline ceramics and nanostructured polycrystalline samples.

Usually, the temperature dependence of the phonon frequency in crystals results from the electron–phonon or phonon–phonon interactions (anharmonicity). Volume-expansion measurements in  $\text{GdCoO}_3$  have revealed the noticeable contribution of the anharmonicity above 1000 K (see below). In this paper, we discuss the measured temperature dependence for  $T < 500$  K, which may be related to the electron–phonon interaction. We show that the local  $\text{CoO}_6$  breathing mode is strongly renormalized by the HS thermally excited states, and the main effect results from the anharmonicity in the local electron–phonon interaction, which is important due to the large ionic-radius difference for HS and LS states.

The structure of the paper is the following: information on the sample preparation and experimental methods is given in Ch.2; experimental data for the structure and optical spectra at different temperatures are given in Ch.3. The data analysis and theoretical interpretation of the temperature-dependent phonon frequency are presented in Ch.4. Ch.5 contains the conclusions.

## 2. Results

The SEM images showed a very broad nanoparticle size distribution (Figure 1). Therefore, for transmission electron microscopy, we used nanoparticles remaining in suspension after exposure to ultrasound; the smallest nanoparticle size, about 10 nm, was obtained for the sample  $\text{GdCoO}_3$  (see Figure 2).

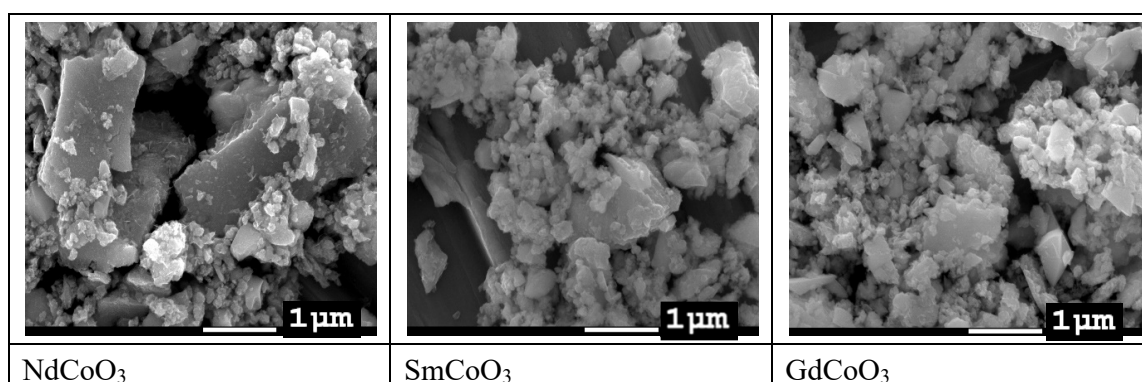


**Figure 1.** SEM images of nanostructured samples after ultrasonic treatment.

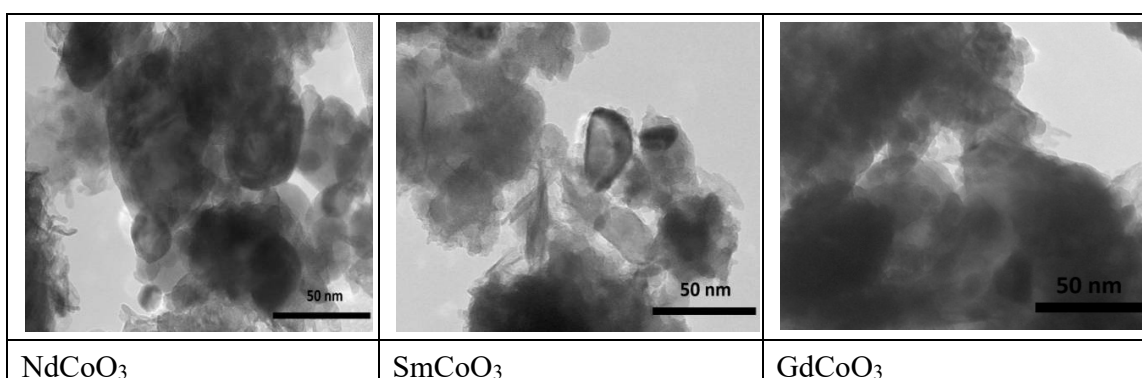


**Figure 2.** Photos from a transmission electron microscope for nanostructured samples after ultrasonic treatment; scale bar, 50 nm.

The optical absorption spectra of  $\text{NdCoO}_3$ ,  $\text{SmCoO}_3$  and  $\text{GdCoO}_3$  at room temperature are shown in the Figure 3 up to the energy 1 eV. The absorption above 0.1 eV is provided by electrons, and in the following, we will restrict ourselves to phonon absorption in the region of energies less than 0.1 eV.

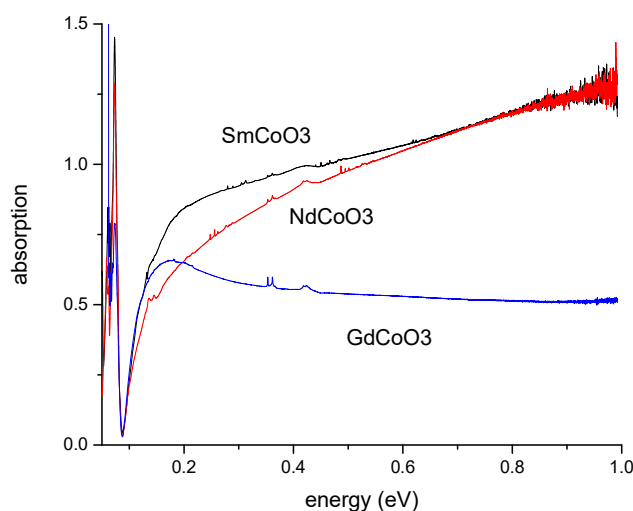


**Figure 3.** The absorption spectra of  $\text{NdCoO}_3$ ,  $\text{SmCoO}_3$  and  $\text{GdCoO}_3$ , measured at  $T = 300$  K.

In this work, we pay special attention to the higher-energy part of the phonon spectrum (0.04–0.08 eV) (see Figures 4 and 5), in which the breathing vibronic mode is located. The high-energy part of the phonon spectrum reveals the well-resolved vibrational excitations, similar to those observed in [15].

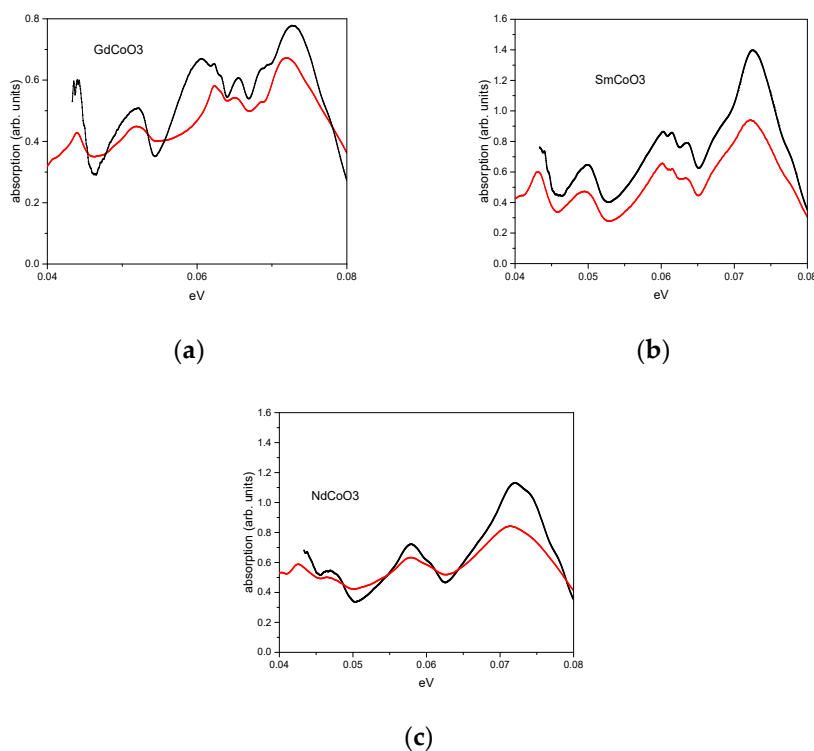


**Figure 4.** Comparison of absorption spectra of nanostructured (red) and polycrystalline (black) samples at room temperature. (a)  $\text{GdCoO}_3$ ; (b)  $\text{SmCoO}_3$ ; (c)  $\text{NdCoO}_3$ .

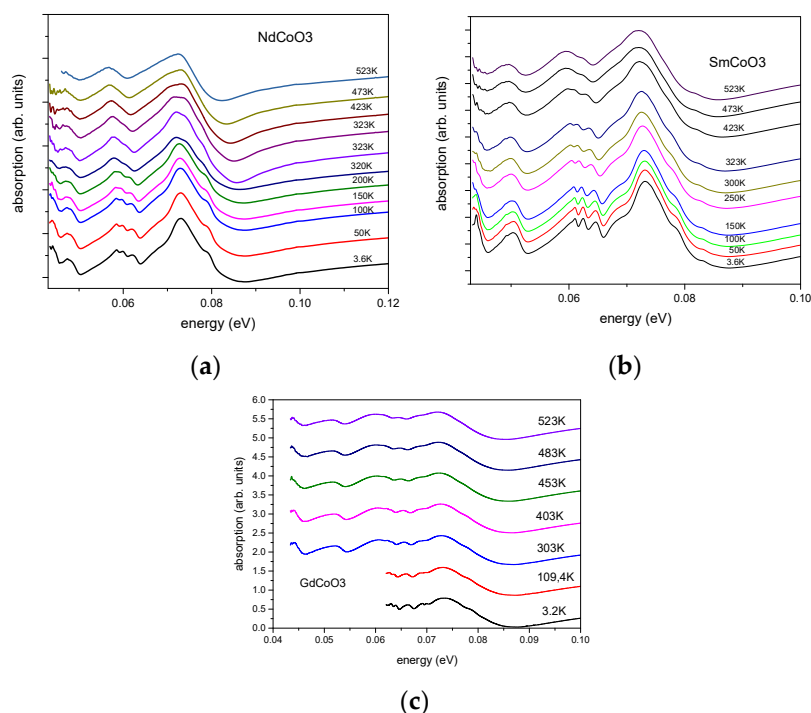


**Figure 5.** Temperature-dependent infrared absorption spectra for NdCoO<sub>3</sub> (a), SmCoO<sub>3</sub> (b) and GdCoO<sub>3</sub> (c).

The comparison of the infrared spectra for the nanostructured and polycrystalline samples in Figure 4 indicated the same energies for the vibronic excitations, close to 0.0725 eV at room temperature. The temperature-dependent phonon-absorption spectra are given in Figure 5, which shows that heating from liquid-helium temperature to 523 K shifts the narrow-peak position by about 73 meV in the direction of decreasing energy.

The highest phonon energy peaks that we associated with the breathing mode (see Ch.4 for a discussion) shift their energy for all three compounds (Figure 6). The shift for Nd is maximal, and that for Gd is minimal.

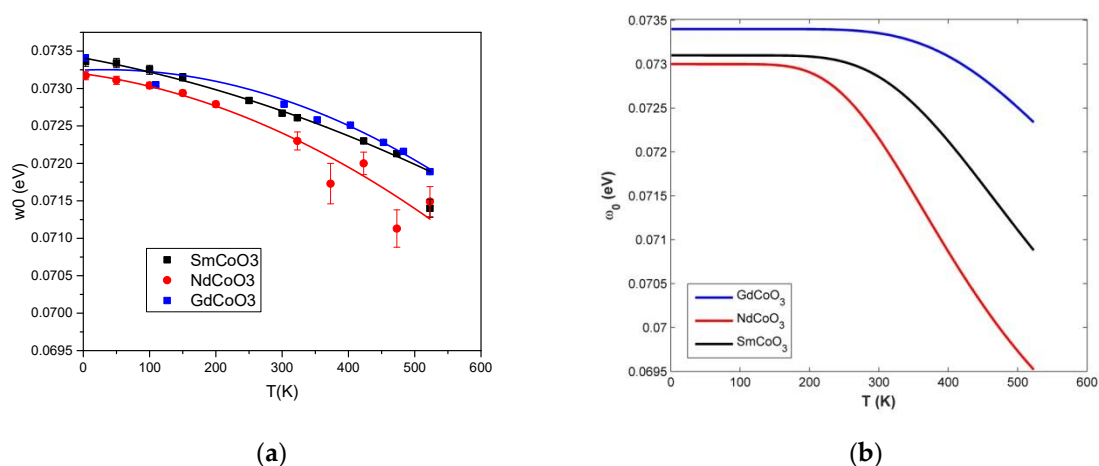


**Figure 6.** The shift of the breathing-mode peak position for different samples depending on temperature measured (a) and calculated in Ch.4 (b). The calculations were performed for the following values of the spin gap  $\Delta_S$ :  $\Delta_{\text{NdCoO}_3} = 1400$  K;  $\Delta_{\text{SmCoO}_3} = 1800$  K;  $\Delta_{\text{GdCoO}_3} = 2300$  K.

### 3. Discussion

#### 3.1. Ab Initio Calculation of Optical Phonons in GdCoO<sub>3</sub>

The optical phonon frequencies were calculated in the framework of the density functional theory (DFT, [16]) implemented in the VASP 5.4.1 program package [17,18]. The exchange–correlation functional of the Perdew–Burke–Ernzerhof formulation [19] was used in combination with the plane-wave basis and the projector-augmented wave (PAW) method [20]. The basis set was limited by the cutoff energy of 520 eV; the integrations over the first Brillouin zone were performed using  $8 \times 8 \times 6$  k-point meshes of the Monkhorst–Pack scheme [21].

The crystal structure of GdCoO<sub>3</sub> in the orthorhombic *Pbnm* phase was fully relaxed to cell size and atom positions; the resulting lattice parameters were  $a = 5.2284$  Å,  $b = 5.4970$  Å and  $c = 7.4805$  Å which agree with previously reported experimental data [12]. The ground state corresponds to low-spin cobalt cations and  $7 \mu_B$  magnetic moments on gadolinium, which are antiferromagnetically ordered (E(FM)–E(AFM) = 1.92 meV/atom). The interatomic force constants were calculated by the finite displacement method within a unit cell and several larger supercells so that the resulting phonon frequencies were converged within 0.05 THz for the calculation cell size. The optical phonon frequencies ( $q = 0$ ) were found using the PHONOPY code [22]. While the CoO<sub>6</sub> octahedra in the *Pbnm* phase are distorted and tilted away from the high-symmetry case, the pure stretching and bending octahedral modes are mixed. To find the breathing mode, all vibration eigenvectors were projected on the direction of uniform elongation of the Co–O bonds. The mode with the highest contribution to the breathing motion (80%) corresponds to the mode of the highest frequency of 17.01 THz. This B<sub>2g</sub> mode corresponds to breathing oscillations of neighboring octahedra in the counter-phase. It is worth noting that the amplitude of the apical oxygen is 84% higher than the amplitudes of the basal atoms, which is connected with the difference in Co–O bond lengths: 1.936 Å and 1.968 Å, respectively.

The vibration modes with frequencies close to the breathing one are B<sub>3g</sub>, counter-phase octahedral stretching (16.54 THz), which is Raman-active as well as a breathing mode [23], and B<sub>2u</sub>, in-phase mixed octahedral bending/stretching (16.28 THz), which is IR-active. The next 19 modes in the range of 13.8–15.9 THz are of stretching and bending natures, with some contribution of Co-atom displacements. The rotational motions of the octahedra appear below a small frequency gap with the B<sub>3g</sub> mode at 11.81 THz. A comparison of the phonon energies measured at  $T = 3.2$  K and those calculated can be seen in Table 1.

**Table 1.** Calculated and measured highest-energy optical phonons for GdCoO<sub>3</sub>.

Mode	B <sub>2u</sub>	B <sub>3g</sub>	B <sub>2g</sub>
Energy, theor., meV	67.3	68.4	70.4
Energy, exper., meV	66.3	68.8	73.3

#### 3.2. Effect of Electron–Phonon Interaction on Temperature Dependence of the Phonon Energy

To describe the effect of multiplicity fluctuations on the phonon-absorption spectrum, we write the Hamiltonian of the electron and phonon subsystems and their interaction in the form:

$$\hat{H} = \sum_i \left( \frac{1}{2} k \hat{q}_i^2 + \frac{\hat{p}_i^2}{2M} \right) - \frac{1}{2} V_q \sum_{\langle i,j \rangle} \hat{q}_i \hat{q}_j - \sum_i (g_1 \hat{q}_i + g_2 \hat{q}_i^2) (\hat{n}_{i,HS} - \hat{n}_{i,LS}) \quad (1)$$

Here, the first term contains the energy of local symmetric vibrations of the cation–anion complex (which we consider as a unit cell and, hereinafter, we will call the SCO complex), while the second and third describe the elastic interaction of cations on neighboring lattice sites and electron–vibron interactions, respectively. The parameters  $g_1$  and  $g_2$  are denoted for linear and quadratic electron–vibron interactions within the SCO complex (MeO<sub>6</sub> octahedra),  $k$  is the elastic coupling constant,  $M$  is the

anion mass,  $\hat{q}$  is the normal coordinate operator of the Me-O breathing vibration,  $\hat{p}$  is the corresponding momentum operator, and  $V_q$  is the parameter of interatomic elastic coupling. The Me-O bond length is equal to  $l = l_0 + \langle \hat{q} \rangle$ , where  $l_0$  is the equilibrium bond length. Since the ionic radii of the cations in the LS and HS states differ quite strongly (the difference is about 10%), it is necessary to take into account not only linear but also quadratic terms in the electron–vibron interaction. For example, in many Fe oxides (Fe<sub>2</sub>O<sub>3</sub>, FeBO<sub>3</sub> etc.), the spin crossover under high pressure at critical value  $P_c \sim 50$  GPa is the first-order phase transition accompanied by the volume change  $\sim 10\%$  [1]. In conventional condensed-matter theory the linear on  $q$  electron–phonon interaction is the harmonic contribution while the quadratic one describes the anharmonicity effects. For example, it contains an emission of two phonons simultaneously in the interaction process [24].

We want to comment on the electron–vibron interaction part; typically, it is given by the product of an oscillator normal coordinate  $\hat{q}$  and electronic density operator  $\hat{n}_e = \sum_p c_p^+ c_p$ , where  $c_p$  ( $c_p^+$ ) are electron-annihilation (creation) operators [25,26]. In our two-level model of the two ionic terms, the HS and the LS, at each cation, the electron-density operator is written via multielectron occupation number operators  $\hat{n}_{i,HS}$  and  $\hat{n}_{i,LS}$ . The mean value  $\langle \hat{n}_{i,HS} \rangle$  gives the probability of the HS term, while  $\langle \hat{n}_{i,LS} \rangle$  provides the probability of the LS state; together,  $\langle \hat{n}_{i,HS} \rangle + \langle \hat{n}_{i,LS} \rangle = 1$ . For the precise definition of these operators, we use the multielectron projection Hubbard  $X$  operators [27,28]. Nevertheless, in this paper, we use the simplest approximation decoupling the anharmonic interaction term  $\hat{q}_i^2 (\hat{n}_{i,HS} - \hat{n}_{i,LS}) \rightarrow \hat{q}_i^2 (\langle \hat{n}_{i,HS} \rangle - \langle \hat{n}_{i,LS} \rangle)$ , so only the HS occupation numbers  $n_{HS} = \langle \hat{n}_{i,HS} \rangle$  and similar  $n_{LS} = \langle \hat{n}_{i,LS} \rangle$  enter the theory. Contrarily, the dynamics under optical pumping require treating the complicated algebra of  $X$  operators [28]. As in the conventional two-level model, these occupation numbers are determined by their energies  $E_{HS}$  and  $E_{LS}$  and degeneracy factors  $m_{HS}$  and  $m_{LS}$ :

$$n_{HS} = \frac{m_{HS} e^{-E_{HS}/k_B T}}{m_{LS} e^{-E_{LS}/k_B T} + m_{HS} e^{-E_{HS}/k_B T}}$$

$$n_{LS} = 1 - n_{HS}.$$

For Co<sup>3+</sup>, the LS state is nondegenerate,  $m_{LS} = 1$ , and the HS state with spin 2 and pseudo-orbital momentum 1 has  $m_{HS} = 15$ . Finally, the difference in the signs of the HS and LS contributions in the electron–vibron interaction reflects the difference in the ionic radii; a more compact LS ion will result in a bond-length contraction, while a larger HS- ion will increase the  $l$  value.

The Hamiltonian (1) in our approximation can be transformed into the form

$$\hat{H} \approx \sum_i \left( \frac{1}{2} [k + 2g_2(1 - 2n_{HS})] \hat{q}_i^2 + \frac{\hat{p}_i^2}{2M} \right) - \frac{1}{2} V_q \sum_{\langle i,j \rangle} \hat{q}_i \hat{q}_j + g_1 (1 - 2n_{HS}) \sum_i \hat{q}_i \quad (2)$$

From Equation (2), it can be seen that the elastic coupling constants in the LS- ( $n_{HS} = 0$ ) and HS- ( $n_{HS} = 1$ ) states are equal to  $k_{LS} = k + 2g_2$  and  $k_{HS} = k - 2g_2$ , respectively; therefore, the frequencies of the local vibrations differ in the HS- and LS- states:  $\omega_{HS} = \sqrt{k_{HS}/M} = \sqrt{(k - 2g_2)/M}$ ;  $\omega_{LS} = \sqrt{k_{LS}/M} = \sqrt{(k + 2g_2)/M}$ . For the selected parameter values from the paper [29] ( $k = 7.5$  eV/Å<sup>2</sup> and  $g_2 = 0.75$  eV/Å<sup>2</sup>), we found  $\omega_{HS} = 0.045$  eV and  $\omega_{LS} = 0.055$  eV. These are the phonon frequencies in the HS and the LS states for a given set of parameters. For the first-order phase transition under high pressure such as for FeBO<sub>3</sub>, one would find the phonon frequency  $\omega_{HS}$  for pressure  $P < P_c$  and the frequency  $\omega_{LS}$  for pressure  $P > P_c$ . The typical shift in the Raman spectra of the order 100 cm<sup>-1</sup> was measured at the spin crossover in Fe<sub>2</sub>O<sub>3</sub> in the paper [30]. Nevertheless, in LnCoO<sub>3</sub>, there is no sharp spin crossover transition with heating at ambient pressure; the LS state is the ground state with a temperature-dependent admixture of the HS state, so the phonon frequency (given below by Equation (5)) is an average with strong red shift. In Figure 7, we demonstrate the smooth evolution of the magnetic properties and volume expansion of GdCoO<sub>3</sub> with heating up to 1300 K.

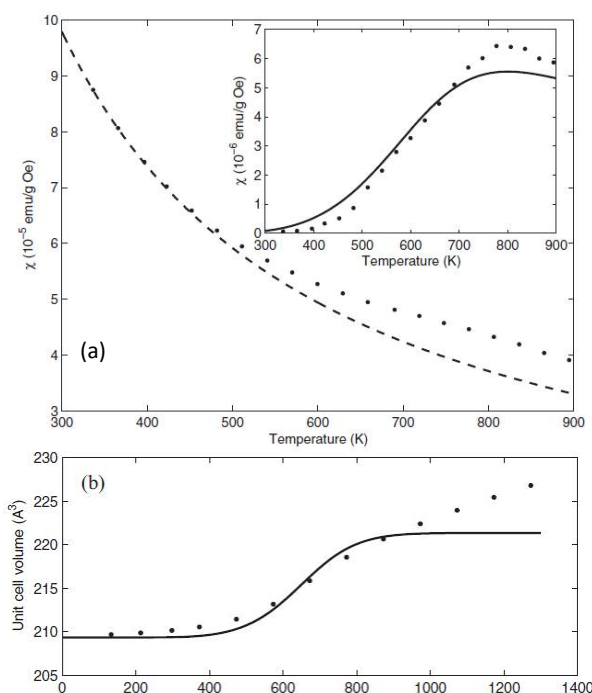


**Figure 7.** The temperature dependence of (a) the magnetic susceptibility; dots show the measured values; the dashed line is for the  $\text{Gd}^{3+}$  Curie–Weiss contribution (with the  $\text{Co}^{3+}$  high-spin (HS) contribution shown by a solid line in the inset, where the difference of the measured and Gd contribution is shown by dots). (b) The volume expansion in  $\text{GdCoO}_3$  from our paper [12]. The solid line in (b) corresponds to the calculated low-spin (LS) volume at low  $T$  and HS volume calculated in harmonic approximation at high  $T$ ; the deviation of the experimental dotted line demonstrates the lattice anharmonicity effect at  $T > 1000$  K.

The Hamiltonian (2) may be written in the form  $\hat{H} = \hat{H}_0 + \hat{H}_1$ , where

$$\hat{H}_0 = \sum_i \left( \frac{1}{2} [k_{LS} - 4g_2 n_{HS}] \hat{q}_i^2 + \frac{\hat{p}_i^2}{2M} \right) - \frac{1}{2} V_q \sum_{\langle i,j \rangle} \hat{q}_i \hat{q}_j \quad (3)$$

$$\hat{H}_1 = g_1 (1 - 2n_{HS}) \sum_i \hat{q}_i \quad (4)$$

With the help of standard canonical transformation [31], we can reduce (3) to the form  $\hat{H}_0 = \sum_k \omega_k (b_k^+ b_k + \frac{1}{2})$ , where for a simple cubic lattice,  $\omega_k = \sqrt{\tilde{\omega}_0^2 \left( 1 - \frac{V_q}{3k} (\cos k_x + \cos k_y + \cos k_z) \right)}$ . Here,  $\tilde{k} = k + 2g_2(1 - 2n_{HS})$ ,

$$\tilde{\omega}_0 = \sqrt{\omega_{LS}^2 - n_{HS} \frac{4g_2}{M}} = \sqrt{\omega_{LS}^2 - n_{HS} \Delta\omega^2} \approx \omega_{LS} - n_{HS} \Delta\omega^2 / 2\omega_{LS} \quad (5)$$

where  $\Delta\omega^2 = (\omega_{LS}^2 - \omega_{HS}^2) \approx 0.001$  eV. For our samples, the LS phonon frequency at  $T = 0$  is about 70 meV, according to Table 1. We should mention that a similar effect of the anharmonicity of the electron–phonon interaction on the optical phonon frequencies has been discussed for the problem of the ferroelectricity in perovskites [32,33], with some hint of high-temperature superconductivity in cuprates [24,34].

Due to the lanthanide contraction, the spin gap value  $\Delta_S = E_{LS} - E_{HS}$  (the energy interval between the LS and HS states) increases with increasing element number for the rare-earth ions [11]. Using Equation (5), we can estimate the effect of multiplicity fluctuations on the phonon-absorption

spectrum with increasing temperature. The right part of Figure 6 shows the calculated temperature dependence of the position of the maximum of the IR absorption spectrum corresponding to the excitation of the breathing mode of the crystal-lattice vibrations for all three compounds. It is seen that the GdCoO<sub>3</sub> sample has the highest value for the spin gap and  $\tilde{\omega}_0$  over the entire temperature range, as a denser medium, due to the smallest ionic radius of the gadolinium ion. As the temperature rises, the absorption maximum shifts to lower frequencies due to increasing high-spin-state occupation (multiplicity fluctuations), which qualitatively corresponds to the obtained experimental data (Figure 6a).

#### 4. Samples and Experimental Methods

The samples LnCoO<sub>3</sub> were obtained with standard ceramic technology using a stoichiometric amount of high-purity oxides Co<sub>3</sub>O<sub>4</sub>, 99.7% (metals basis, Sigma-Aldrich, St. Louis, MO, USA) and Ln<sub>2</sub>O<sub>3</sub> (Ln = Nd, Sm, Gd), 99.99% (Rare Metals Plant, Novosibirsk, Russia). To obtain samples with a grain size of 20 to 50 μm, the initial compositions were thoroughly mixed in an agate mortar using ethanol, annealed in air at a temperature of  $T = 1373$  K in a corundum crucible for 24 h with a triple grinding–calcining cycle and cooled together with the furnace to room temperature at a speed of 2 K/min. After annealing, the mixture was ground again; tablets were pressed into bars of  $5 \times 13 \times 2$  mm<sup>3</sup>, which were then annealed in air at a temperature of 1473 K for 8 h, cooled and ground for measurements.

Additionally, nanoscale samples were prepared to investigate the effect of particle size on optical properties. Powders with a grain size of less than 100 nm were obtained by wet grinding in deionized water using a Pulverisette 7 premium-line planetary micro mill (Fritsch GmbH, Idar-Oberstein, Germany) in two stages. In the first stage, a powder with a grain size of 20 to 50 μm was loaded into a zirconium dioxide (96.2% ZrO<sub>2</sub>) milling bowl with ZrO<sub>2</sub> balls 3 mm in diameter and milled for 150 min at 800 rpm. Furthermore, additional grinding was carried out for 30 min at 1100 rpm. After evaporation, the resulting powder was placed in an ultrasonic bath and crushed in ethyl alcohol for 5 min.

Powder X-ray diffraction (PXRD) data for the polycrystalline samples have been discussed recently in [14]. Here, we also present the electron microscopy data. The elemental analysis was carried out with a scanning electron microscope (SEM) with an X-ray spectroscopy detector (EDX, Hitachi TM 3000). The study of the sample's structural properties was carried out using transmission electron microscopy (TEM) using a Hitachi HT7700 microscope at an accelerating voltage of 100 kV.

The morphology of the samples was investigated with SEM with a JEOL JSM-7001F electron microscope operating at 15 kV. For these measurements, the nanoparticle powder was placed in ethanol and subjected to ultrasonic treatment for 5 min.

In this paper, we measured the NdCoO<sub>3</sub>, SmCoO<sub>3</sub> and GdCoO<sub>3</sub> absorption spectra in the infrared (IR) region at temperatures from 3.2 to 523 K. The IR spectroscopy measurements were carried out with the vacuum Fourier Transformation IR spectrometer Vertex 80 v equipped with an RT-DLaTGS detector. Cryogenic measurements were carried out with a cryostat-type OptistatAC-V12 and Temperature Controller ITC503s from Oxford Instruments in the range 3.2–296 K. For the temperature region 297–523 K, we used a Variable Temperature Cell 147/QV High Stability Temperature Controller 4000 Series TM from Specac Ltd. The sample was prepared by mixing 0.200 g of KBr powder and 0.001 g of crystal mass, to be pressed into a tablet of diameter 13 mm.

#### 5. Conclusions

We have demonstrated, experimentally, an unusually strong softening of the optical phonon mode, and we have theoretically related it to fluctuations of the multiplicity that result in a thermally induced partial occupation of the high-spin terms. In the row NdCoO<sub>3</sub>, SmCoO<sub>3</sub> and GdCoO<sub>3</sub>, the spin-gap value increases [11], where the increase in the HS concentration is the largest for NdCoO<sub>3</sub> and the smallest for GdCoO<sub>3</sub>. This large phonon-energy shift results from the anharmonic contribution in



the electron–phonon interaction. While all the effects of anharmonicity in the lattice are usually related with very high temperature, here, we have revealed that the fluctuations of multiplicity in the electronic system due to anharmonic electron–phonon interaction results in a quite noticeable effect at the moderate temperatures of 300–500 K due to small spin-gap values.

Contrary to other materials with SCO with a sharp switching between HS and LS states under high pressure or heating [2–4], the rare-earth cobaltites demonstrate a smooth increase in the HS population due to the multiplicity fluctuations.

**Author Contributions:** Conceptualization, S.G.O.; Methodology, Y.S.O. and M.A.V.; Data Curation, Y.S.O. and M.A.V.; Investigation, A.E.S., V.A.D., K.V.S., M.N.V., S.M.Z. and N.P.S.; Writing–Original Draft Preparation, S.G.O.; Writing–Review and Editing, Y.S.O. and M.A.V.; Project Administration, S.G.O.; Supervision, S.G.O.; Funding Acquisition, S.G.O. All authors have read and agreed to the published version of the manuscript.

**Funding:** This work was supported by the Russian Science Foundation grant 18-02-00022. The scanning electron microscopy investigations were conducted in the SFU Joint Scientific Center, supported by the State assignment (#FSRZ-2020-0011) of the Ministry of Science and Higher Education of the Russian Federation. The other research was carried out at the Krasnoyarsk Regional Center of Research Equipment of the Federal Research Center “Krasnoyarsk Science Center SB RAS”.

**Conflicts of Interest:** The authors declare no conflict of interest.

## References

1. Lyubutin, I.S.; Gavriulik, A.G. Research on phase transformations in 3d-metal oxides at high and ultrahigh pressure: State of the art. *Phys. Usp.* **2009**, *52*, 989–1017. [[CrossRef](#)]
2. Gülich, P.; Goodwin, H.A. *Spin Crossover in Transition Metal Compounds I–III*; Springer: Berlin/Heidelberg, Germany, 2004.
3. Halcrow, M.A. *Spin-Crossover Materials: Properties and Applications*; John Wiley & Sons, Ltd.: Oxford, UK, 2013.
4. Aromi, G.; Real, J.A. Special Issue “Spin Crossover Research”. *Magnetochemistry* **2016**, *2*, 28. [[CrossRef](#)]
5. Kitazawa, T. Special Issue “Synthesis and applications of New Spin Crossover Compounds”. *Crystals* **2019**, *9*, 382. [[CrossRef](#)]
6. Raccah, P.M.; Goodenough, J.B. First-order localized-electron  $\leftrightarrow$  Collective-electron transition in LaCoO<sub>3</sub>. *Phys. Rev.* **1967**, *155*, 932–943. [[CrossRef](#)]
7. Bhide, V.G.; Rajoria, D.S. Mössbauer studies of the high-spin-low-spin equilibria and the localized collective electron transition in LaCoO<sub>3</sub>. *Phys. Rev. B* **1972**, *6*, 1021–1032. [[CrossRef](#)]
8. Knížek, K.; Jirak, Z.; Hejtmanek, J.; Veverka, M.; Marysko, M.; Maris, G.; Palstra, T.T.M. Structural anomalies associated with the electronic and spin transitions in LnCoO<sub>3</sub>. *Eur. Phys. J. B Condens. Matter Complex Syst.* **2005**, *47*, 213–220. [[CrossRef](#)]
9. Alonso, J.A.; Martinez-Lope, M.J.; de la Calle, C.; Pomjakushin, V. Preparation and structural study from neutron diffraction data of RCoO<sub>3</sub> (R = Pr, Tb, Dy, Ho, Er, Tm, Yb, Lu) perovskites. *J. Mater. Chem.* **2006**, *16*, 1555–1560. [[CrossRef](#)]
10. Berggold, K.; Kriener, M.; Becker, P.; Benomar, M.; Reuther, M.; Zobel, C.; Lorenz, T. Anomalous expansion and phonon damping due to the Co spin-state transition in RCoO<sub>3</sub> (R = La, Pr, Nd, and Eu). *Phys. Rev. B* **2008**, *78*, 134402. [[CrossRef](#)]
11. Ovchinnikov, S.G.; Orlov, Y.S.; Dudnikov, V.A. Temperature and Field Dependent Electronic Structure and Magnetic Properties of LaCoO<sub>3</sub> and GdCoO<sub>3</sub>. *J. Magn. Magn. Mater.* **2012**, *324*, 3584–3587. [[CrossRef](#)]
12. Orlov, Y.S.; Solovyov, L.A.; Dudnikov, V.A.; Fedorov, A.S.; Kuzubov, A.A.; Kazak, N.V.; Voronov, V.N.; Vereshchagin, S.N.; Shishkina, N.N.; Perov, N.S.; et al. Structural properties and high-temperature spin and electronic transitions in GdCoO<sub>3</sub>: Experiment and theory. *Phys. Rev. B* **2013**, *88*, 235105. [[CrossRef](#)]
13. Dudnikov, V.A.; Orlov, Y.S.; Kazak, N.V.; Platunov, M.S.; Ovchinnikov, S.G. Anomalies of the electronic structure and physical properties of rare-earth cobaltites near spin crossover. *JETP Lett.* **2016**, *104*, 588. [[CrossRef](#)]
14. Dudnikov, V.A.; Orlov, Y.S.; Solovyov, L.A.; Vereshchagin, S.N.; Gavrilkin, S.Y.; Tsvetkov, A.Y.; Velikanov, D.A.; Gorev, M.V.; Novikov, S.V.; Ovchinnikov, S.G. Effect of Multiplicity Fluctuation in Cobalt Ions on Crystal Structure, Magnetic and Electrical Properties of NdCoO<sub>3</sub> and SmCoO<sub>3</sub>. *Molecules* **2020**, *25*, 1301. [[CrossRef](#)] [[PubMed](#)]
15. Kim, Y.Y.; Lee, D.H.; Kwon, T.Y.; Park, S.H. Infrared Spectra and Seebeck Coefficient of LnCoO<sub>3</sub> with the Perovskite Structure. *J. Sol. State Chem.* **1994**, *112*, 376. [[CrossRef](#)]

16. Hohenberg, P.; Kohn, W. Density functional theory (DFT). *Phys. Rev.* **1964**, *136*, B864. [[CrossRef](#)]
17. Kresse, G.; Hafner, J. Ab initio molecular dynamics for liquid metals. *Phys. Rev. B* **1993**, *47*, 558. [[CrossRef](#)]
18. Kresse, G.; Furthmüller, J. Efficient iterative schemes for ab initio total-energy calculations using a plane-wave basis set. *Phys. Rev. B* **1996**, *54*, 11169. [[CrossRef](#)]
19. Perdew, J.P.; Burke, K.; Ernzerhof, M. Generalized gradient approximation made simple. *Phys. Rev. Lett.* **1996**, *77*, 3865. [[CrossRef](#)]
20. Blöchl, P.E. Projector augmented-wave method. *Phys. Rev. B* **1994**, *50*, 17953. [[CrossRef](#)]
21. Monkhorst, H.J.; Pack, J.D. Special points for Brillouin-zone integrations. *Phys. Rev. B* **1976**, *13*, 5188. [[CrossRef](#)]
22. Togo, A.; Tanaka, I. First principles phonon calculations in materials science. *Scr. Mater.* **2015**, *108*, 1–5. [[CrossRef](#)]
23. Nakamoto, K. *Infrared and Raman Spectra of Inorganic and Coordination Compounds, Part A: Theory and Applications in Inorganic Chemistry*, 6th ed.; John Wiley & Sons: Hoboken, NJ, USA, 2009.
24. Bussmann-Holder, A. Ferroelectricity and superconductivity: Two competing phenomena. *Ferroelectrics* **1993**, *144*, 173. [[CrossRef](#)]
25. Lipari, N.O.; Duke, C.B.; Pietronero, L. Electron–vibration interactions in benzene and deuterobenzene. *J. Chem. Phys.* **1976**, *65*, 1165. [[CrossRef](#)]
26. Painelli, A.; Girlando, A. Electron–molecular vibration (e–mv) coupling in charge-transfer compounds and its consequences on the optical spectra: A theoretical framework. *J. Chem. Phys.* **1986**, *84*, 5655. [[CrossRef](#)]
27. Ovchinnikov, S.G.; Val'kov, V.V. *Hubbard Operators in the Theory of Strongly Correlated Electrons*; Imperial College Press: London, UK, 2004.
28. Orlov, Y.S.; Nikolaev, S.V.; Ovchinnikov, S.G.; Nesterov, A.I. Ultrafast quantum dynamics of relaxation in magnetic system with spin crossover under the sudden excitation. *JETP Lett.* **2020**, *112*, 268–274.
29. D'Avino, G.; Painelli, A.; Boukheddaden, K. Vibronic model for spin crossover complexes. *Phys. Rev. B* **2011**, *84*, 104119. [[CrossRef](#)]
30. Shim, S.-H.; Duffy, T.S. Raman spectroscopy of Fe<sub>2</sub>O<sub>3</sub> to 62 GPa. *Am. Mineral.* **2002**, *87*, 318–326. [[CrossRef](#)]
31. Mattuck, R.D. *A Guide to Feynman Diagrams in the Many-Body Problem*, 2nd ed.; McGraw-Hill: New York, NY, USA, 1976.
32. Migoni, R.; Bilz, H.; Bauerle, D. Origin of Raman Scattering and Ferroelectricity in Oxidic Perovskites. *Phys. Rev. Lett.* **1976**, *37*, 1155. [[CrossRef](#)]
33. Bilz, H.; Bedenek, G.; Bussmann-Holder, A. Theory of ferroelectricity: The polarizability model. *Phys. Rev. B* **1987**, *35*, 4840. [[CrossRef](#)]
34. Bussmann-Holder, A.; Simon, A.; Buttner, H. Possibility of a common origin to ferroelectricity and superconductivity in oxides. *Phys. Rev. B* **1989**, *39*, 207. [[CrossRef](#)]

**Sample Availability:** Samples of the compounds are not available from the authors.



© 2020 by the authors. Licensee MDPI, Basel, Switzerland. This article is an open access article distributed under the terms and conditions of the Creative Commons Attribution (CC BY) license (<http://creativecommons.org/licenses/by/4.0/>).